Langmuir

Article

pubs.acs.org/Langmuir

Formation of Au–Pt Alloy Nanoparticles on a Si Substrate by Simple Dip-Coating at Room Temperature

Liyan Zhao, Nina Heinig, and K. T. Leung*

WATLab and Department of Chemistry, University of Waterloo, Waterloo, Ontario, Canada N2L 3G1

ABSTRACT: Spherical Au–Pt alloy nanoparticles of 10 nm average size have been prepared on a H-terminated Si(100) substrate by an extremely simple method of dip-coating. X-ray photoelectron spectroscopy and glancing-incidence X-ray diffraction confirm the formation of Au–Pt alloy. The Au^{3+} ions are first reduced on the Si substrate upon dipping, and the freshly formed Au nuclei then work as a "catalyst" by promoting the reduction of $PtCl_6^{2-}$ ions on the Au nuclei. The subsequent interdiffusion of Au and Pt atoms leads to the observed alloy formation. The present method provides an environment-friendly, low-cost route to preparing anode electrodes in fuel cells.

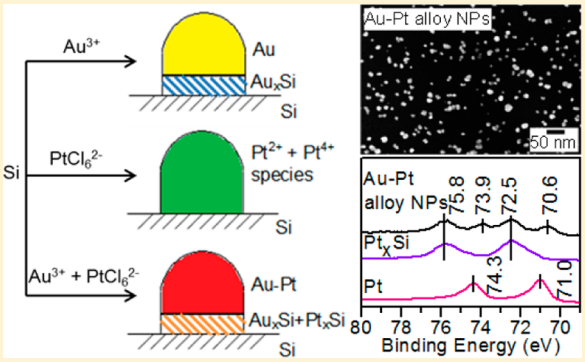

1. INTRODUCTION

Au–Pt alloy nanoparticles (NPs) are of great importance because they are used as common electrocatalysts, selective oxidants, and dehydrogenation catalysts.[1−6] It is well-known that the synthesis of single-phase Au–Pt alloy is a big challenge because Au and Pt are immiscible in the bulk.[7] However, theoretical calculations of the heats of formation for Au–Pt alloy nanoparticles suggested that Au–Pt alloy could be prepared as nanoscale materials.[8] Au–Pt alloy NPs are usually obtained by simultaneous reduction of the respective metal salt precursors by using reducing agents. For example, Schrinner et al. prepared Au–Pt alloy NPs[9] by first immobilizing $[AuCl_4]^-$ ions on spherical polyelectrolyte brushes followed by ultrafiltration to remove the excess ions. This was then followed by immobilizing $[PtCl_6]^{2-}$ ions with further ultrafiltration and finally reduction of these immobilized $[AuCl_4]^-$ and $[PtCl_6]^{2-}$ ions by $NaBH_4$. The formation of a true solid solution in these ultrasmall Au–Pt alloy NPs of various compositions (1.8–4.0 nm in diameter) was confirmed by wide-angle X-ray scattering. Xu et al. obtained near-spherical $Au_{50}Pt_{50}$ alloy NPs with a narrow size distribution of 3.0–4.8 nm, by coreduction of Au and Pt ions in an *N*,*N*-dimethylformamide coordinated Au^{3+}–Pt^{4+} precursor complex.[10] The Au–Pt alloy formation was also verified by X-ray diffraction (XRD) and high-resolution transmission electron microscopy. Habrioux et al. prepared carbon-supported Au–Pt alloy NPs by mixing two water-in-oil microemulsions (of ultrapure water–tetraethylene glycol and monododecyl ether–*n*-heptane with the same composition), with one containing the precursor salts ($HAuCl_4$ + H_2PtCl_6) and the other a reducing agent ($NaBH_4$). After formation of Au–Pt alloy NPs in the microemulsion, an appropriate amount of carbon black (Vulcan XC-72R) was added under constant stirring for 2 h. The supported Au–Pt alloy NPs were separated, washed several times with acetone, ethanol, and ultrapure water to eliminate excess surfactants, and finally dried in vacuum.[11] Recently, Essinger-Hileman et al. also prepared Au–Pt alloy NPs by slowly adding a coreduction agent, $NaBH_4$, into the aqueous metal salt ($HAuCl_4$ + K_2PtCl_4) solution with polyethylene glycol as a surface stabilizer. This was then followed by constant stirring for over 1 h, and the resulting particles were collected by centrifugation and washed several times with ethanol.[12] All these earlier studies illustrate the challenges and complexities in the multistep procedures used in preparing Au–Pt alloy NPs. In contrast, here we prepare the Au–Pt alloy NPs by simply dipping our H-terminated Si substrate into an aqueous solution containing $AuCl_3$ and $PtCl_4$. The present approach is the simplest method ever reported for preparing Au–Pt alloy NPs. As the working solution is just an aqueous solution of inorganic salts of $AuCl_3$ and $PtCl_4$, the present method is also environmentally safe without the need for a massive amount of organic solvents. The dipping method is also free of surfactants, which were needed and coated on top of the as-prepared Au–Pt alloy NPs to prevent coagulation in the earlier work,[11] and is therefore free of any undesirable effect introduced by the surfactants on the catalytic properties of these alloys.

2. EXPERIMENTAL DETAILS

The Au–Pt alloy NPs are deposited on single-side-polished, p-type Si(100) chips (15 × 2.5 mm^2, 0.525 mm thick), with a resistivity of 10–20 mΩ·cm, that have been hydrogen-terminated by using a standard procedure. Si(100) chips are cleaned by using the RCA (Radio Corporation of America) method. This Si cleaning method consists of two steps: The Si chip is first immersed in a solution of ammonium hydroxide, hydrogen peroxide, and deionized water

Received: May 27, 2012
Revised: December 8, 2012
Published: December 12, 2012

(resistivity of 18.2 MΩ·cm) in a 1:1:5 ratio at 70 °C for 15 min to remove organic residues and then in a solution of hydrochloric acid, hydrogen peroxide, and deionized water in a 1:1:5 ratio at 70 °C for 15 min to remove metallic residues. Vigorous rinsing with deionized water is performed after each of these steps. Finally, the Si chips are H-terminated by etching in an aqueous HF (2%) solution to remove the native oxide layer and rinsed thoroughly with deionized water.[13] The clean H-terminated Si(100) chips are then dipped in a solution containing 1 mM $AuCl_3$ and/or 1 mM $PtCl_4$ for 10 min. To compare the electrodeposition result of Au−Pt alloy NPs reported elsewhere,[14] we also add 100 mM $NaClO_4$ to the solution of 1 mM $AuCl_3$ and 1 mM $PtCl_4$, and the results for the dipping experiments are found to be the same. After dipping, the Si(100) chips are thoroughly rinsed with deionized water and dried in N_2 before further analysis. We have also used Si(100) chips without RCA cleaning and found that the Si substrate with a native oxide layer could also be used to obtain Au−Pt alloy NPs but with less uniformity. The surface morphology of the resulting deposits is characterized by scanning electron microscopy (SEM) with a LEO 1530 field-emission scanning electron microscope. The corresponding chemical-state composition is analyzed by X-ray photoelectron spectroscopy (XPS) as a function of the argon ion sputtering time with a Thermo-VG Scientific ESCALab 250 microprobe equipped with a monochromatic Al Kα X-ray source (1486.6 eV), at a typical energy resolution of 0.4−0.5 eV full width at half-maximum (fwhm). Argon ion sputtering is performed over a rastered area of 3 × 3 mm^2 of the sample at an ion beam energy of 3 keV and a typical sample current density of 110 nA mm^{-2}. The crystal structures of the nanodeposits are determined by glancing-incidence XRD (GIXRD) at an incidence angle of 0.6°, using a PANalytical MRD X'pert Pro diffractometer with the Cu Kα anode operating at 45 kV and 35 mA. The electrocatalytic activity of the nanodeposits is characterized by performing cyclic voltammetry (CV) measurements in a three-electrode cell with a CH Instruments 660A potentio/galvanostat electrochemical workstation. A standard Ag/AgCl reference electrode and a platinum-wire counter electrode are used. All the electrolytic solutions are deoxygenated with high-purity nitrogen gas before the CV measurement.

3. RESULTS AND DISCUSSION

The surface morphology of the Si chip obtained by dipping in a solution of 1 mM $AuCl_3$ and 1 mM $PtCl_4$ (pH 2.85) for 10 min is shown in Figure 1a. Spherical NPs with an average diameter of 10 nm (with a standard deviation of 4.5 nm) are obtained (Figure 1b). The GIXRD pattern (Figure 1c) exhibits eight major peaks that can be assigned to the face-centered cubic lattice of Au−Pt alloy. The shifts of the (111) peak to a higher 2θ angle (0.11° shift) from pure Au (JCPDS 04-0784) and to a lower 2θ angle (1.58° shift) from pure Pt (JCPDS 04-0802) indicate a single-phase Au−Pt alloy. For comparison, the GIXRD pattern of a pristine Au foil (measured in the same setup) is also shown in Figure 1c. The shift of the (111) plane for the Au−Pt alloy is evident, while the much broader peak is due to the small particle size. Using 2θ of the (111) peak at 38.29°, we estimate the lattice constant for the fcc-type Au−Pt alloy NPs to be 4.068 Å, which corresponds to a calculated composition of $Au_{93}Pt_7$ according to Vegard's law.[15] According to the Scherrer equation (with a Scherrer constant of 0.9),[16] the crystallite size of the Au−Pt alloy NPs as estimated from the fwhm of the (111) diffraction peak is 11 nm, which is in excellent accord with our SEM measurement (Figure 1a). The features at 50−60° are found to correspond to the (311) plane of the p-Si(100) substrate reported in the literature.[17]

The corresponding XPS depth-profiling spectra in the Au 4f and Pt 4f regions of the Au−Pt NPs are shown in parts a and b, respectively, of Figure 2. To determine the binding energy reference spectra for metallic Au and Pt (with a film thickness

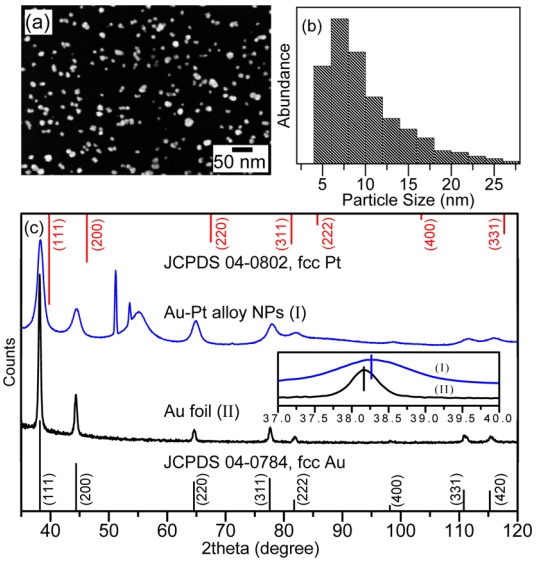

Figure 1. (a) SEM image, (b) size distribution, and (c) GIXRD pattern of Au−Pt alloy nanoparticles obtained by dipping a H-terminated Si(100) substrate in a solution of 1 mM $AuCl_3$ and 1 mM $PtCl_4$ for 10 min. The GIXRD pattern of a Au foil and the reference patterns JCPDS 04-0784 for fcc Au (bottom bar chart) and JCPDS 04-0802 for fcc Pt (top bar chart) are also shown in (c). The inset shows the small shift of 2θ of the (111) diffraction features between the Au−Pt alloy NPs and Au foil samples.

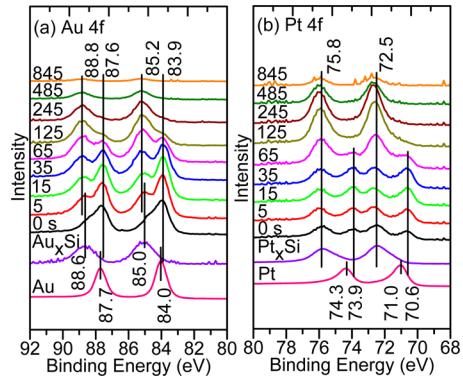

Figure 2. Depth-profiling XPS spectra of (a) Au 4f and (b) Pt 4f regions of Au−Pt alloy nanoparticles obtained by dipping a H-terminated Si substrate in a solution of 1 mM $AuCl_3$ and 1 mM $PtCl_4$ for 10 min. XPS spectra corresponding to metallic Au and Pt and to Au_xSi and Pt_xSi from magnetron-sputtered Au and Pt films with the appropriate thicknesses are provided as references.

of 200 nm) and for gold silicide (Au_xSi) and platinum silicide (Pt_xSi) (with a film thickness of 1 nm), we also deposit Au and Pt films with appropriate thicknesses on H-terminated Si chips by magnetron sputtering. These XPS spectra are also shown and compared with those of Au−Pt NPs in Figure 2. For the as-prepared NPs, the prominent Au $4f_{7/2}$ ($4f_{5/2}$) feature at 83.9 eV (87.6 eV) is discernibly broader than that obtained for a metallic Au film, while the shoulder at 85.0 eV is indicative of the formation of Au_xSi. Two Pt $4f_{7/2}$ ($4f_{5/2}$) features at 70.6 eV (73.9 eV) and 72.5 eV (76.0 eV) are also observed, with the former shifted from the metallic film position by 0.4 eV and the latter attributable to Pt_xSi. Both the Au $4f_{7/2}$ feature at 83.9 eV and the Pt $4f_{7/2}$ feature at 70.6 eV are found to be 0.1 and 0.4 eV lower than the respective features for metallic Au (84.0 eV) and Pt (71.0 eV). These observed shifts indicate the presence

dx.doi.org/10.1021/la303809m | Langmuir 2013, 29, 927−931

of alloy in the NPs. On the basis of the atomic ratio of Au to Pt for the alloy (18.4), calculated from the XPS peak intensities appropriately scaled by the respective atomic sensitivity factors, we conclude that the as-prepared alloy corresponds to $Au_{95}Pt_5$, in good accord with that obtained by GIXRD ($Au_{93}Pt_7$). It should be noted that both the Au $4f_{7/2}$ and Pt $4f_{7/2}$ features exhibit negative binding energy shifts from those of metallic Au and Pt, which have also been reported in other studies.[18−20] These shifts (without any Argon sputtering) could be the result of Au−Pt alloy formation, and they have also been found by calculations using the local density functional method within the initial state approximation.[18] Upon sputtering for 5 s, a well-defined Au $4f_{7/2}$ ($4f_{5/2}$) peak at 85.0 eV (88.6 eV) emerges (from the shoulder) and is assigned to Au_xSi. Further sputtering to 245 s appears to completely remove the Au 4f and Pt 4f features attributable to the Au−Pt alloy. The small shifts in the binding energies for the Au_xSi and Pt_xSi features (less than 0.2 eV) could also be the result of minor composition changes in the interface. Further sputtering for 845 s totally removes the remaining Au_xSi and Pt_xSi features. XPS depth profiling is used only to investigate the interface between the Au−Pt alloy NPs and Si surface. Argon ion sputtering does not introduce any binding energy shift for the alloy components either. To exclude the argon ion sputtering effect (of altering the chemistry of the surface species), we perform, in separate experiments, aggressive argon sputtering on metallic Au and metallic Pt films (which we deposit on Si) for over 15 min, and no binding energy shift is observed.

To investigate the mechanism of the Au−Pt alloy formation, we also dip an ITO-glass (ITO = indium tin oxide) substrate in the same aqueous solution containing 1 mM $AuCl_3$ and 1 mM $PtCl_4$ for 10 min, and the corresponding Au 4f and Pt 4f spectra are compared with those for the samples prepared by dipping Si substrate in Figure 3. On the ITO-glass substrate, a Au $4f_{7/2}$ ($4f_{5/2}$) feature is found at 84.4 eV (88.0 eV) (Figure 3a), indicating the formation of the Au^+ form,[21] while the Pt $4f_{7/2}$ ($4f_{5/2}$) feature at 73.3 eV (76.6 eV) (Figure 3b), found between

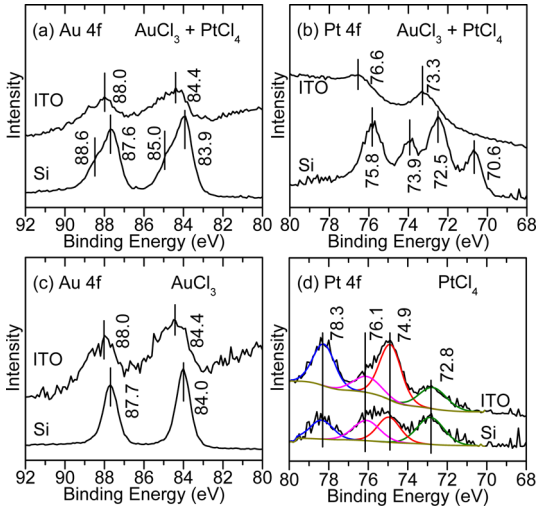

Figure 3. (a) Au 4f and (b) Pt 4f regions of the samples obtained by dipping a H-terminated Si substrate and an ITO-glass substrate in a solution of 1 mM $AuCl_3$ and 1 mM $PtCl_4$ for 10 min. (c) Au 4f region of the samples obtained by dipping a H-terminated Si substrate and an ITO-glass substrate in 1 mM $AuCl_3$ solution for 10 min. (d) Pt 4f region for the samples obtained by dipping a H-terminated Si substrate and an ITO-glass substrate in 1 mM $PtCl_4$ solution for 10 min.

the Pt^{4+} and Pt^{2+} oxidation states, suggests the formation of a possible bimetallic Au−Pt complex. No Au−Pt alloy formation is therefore observed on the ITO-glass substrate, in contrast to the Si substrate. In our earlier work, we demonstrated that dipping a H-terminated Si(100) substrate in a solution of $AuCl_3$ and 100 mM $NaClO_4$ produces metallic Au NPs, with Au_xSi formed at the interface between the Au NPs and Si substrate.[22] We have now performed the same dipping experiment on an ITO-glass substrate and observe the Au $4f_{7/2}$ ($4f_{5/2}$) feature at 84.4 eV (88.0 eV) (Figure 3c), i.e., the same position as that found for dipping in a solution of $AuCl_3$ and $PtCl_4$ (Figure 3a). This shows that only a species with Au^+ is found on the ITO-glass substrate (Figure 3c), in contrast to the metallic Au, with a characterisitic Au $4f_{7/2}$ ($4f_{5/2}$) feature at 84.0 eV (87.7 eV), found on the H-terminated Si(100) substrate (Figure 3c). In a separate experiment, we obtain, by dipping a H-terminated Si(100) or an ITO-glass substrate in 1 mM $PtCl_4$ solution for 10 min, nanodeposits with Pt $4f_{7/2}$ ($4f_{5/2}$) features at 72.8 eV (76.1 eV) and 74.9 eV (78.3 eV) binding energy, corresponding to Pt^{2+} and Pt^{4+} species,[23] respectively (Figure 3d). Together with the Cl 2p peak found in the survey spectrum (not shown), this suggests adsorption of insoluble platinum salt onto the H-terminated Si(100) or ITO substrate and partial reduction from the Pt^{4+} state to the Pt^{2+} state. It is important to emphasize that dipping in a solution containing just $PtCl_4$ does not produce metallic Pt NPs on a H-terminated Si(100) substrate. However, in a solution containing both $PtCl_4$ and $AuCl_3$, we obtain a metallic Pt nanodeposit, part of which is converted to Au−Pt alloy, while the remaining reacts with Si to form Pt_xSi at the interface. This phenomenon, shown schematically in Figure 4,

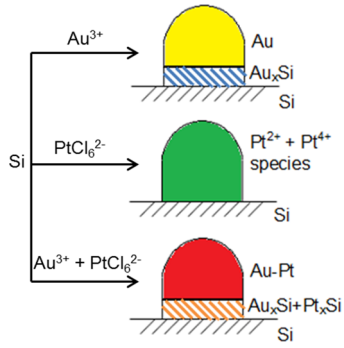

Figure 4. Schematic models of the as-prepared samples by dipping a H-terminated Si substrate in various solutions involving $AuCl_3$, $PtCl_4$, and $AuCl_3$ + $PtCl_4$.

could be explained by the following mechanism. In an aqueous solution of 1 mM $AuCl_3$ and 1 mM $PtCl_4$ (pH 2.85), $AuCl_3$ is dissolved into Au^{3+} and Cl^- ions while $PtCl_4$ is present in the form of a $PtCl_6^{2-}$ complex in acidic media due to the reaction $PtCl_4(s) + 2Cl^-(aq) \rightarrow PtCl_6^{2-}(aq)$.[24] The Au^{3+} ions are first reduced on the Si substrate upon electroless deposition (as discussed in our earlier work),[22] and the freshly formed Au nuclei then work as a "catalyst" by promoting reduction of $PtCl_6^{2-}$ ions on top of the Au nuclei. The subsequent interdiffusion of Au and Pt atoms then leads to the observed alloy formation. The presence of $AuCl_3$ in $PtCl_4$ is therefore vitally important in this simple method of synthesizing the Au−Pt alloy nanoparticles. Since dipping ITO-glass into a $AuCl_3$ solution does not produce metallic Au nuclei, dipping ITO-glass into a solution of $AuCl_3$ and $PtCl_4$ will not lead to Au catalysts to promote the formation of metallic Pt. Au−Pt alloy

dx.doi.org/10.1021/la303809m | Langmuir 2013, 29, 927−931

is only found on the surface of Si instead of ITO-glass because H-terminated Si(100) can be oxidized to SiO_x, which provides the electrons first for the reduction of Au^{3+} and then for the reduction of $PtCl_6^{2-}$ ions, with Au nuclei acting as the catalysts. To further verify our proposed mechanism, we also (in separate experiments) sequentially dipped the H-terminated Si(100) substrate, first for 10 s in 1 mM $AuCl_3$ solution and then for 10 min in 1 mM $PtCl_4$ solution. The as-prepared sample reveals the Au $4f_{7/2}$ ($4f_{5/2}$) alloy feature at 83.9 eV (87.6 eV) and Pt $4f_{7/2}$ ($4f_{5/2}$) alloy feature at 70.6 eV (74.0 eV) (Figure 5), which

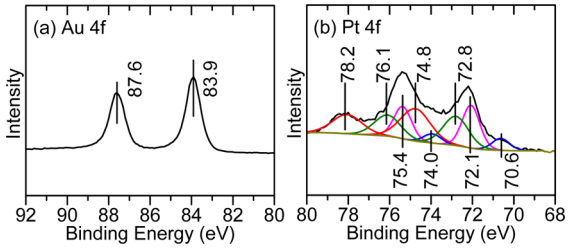

Figure 5. XPS spectra of (a) Au 4f and (b) Pt 4f regions for nanoparticles obtained by dipping a H-terminated Si substrate first in 1 mM $AuCl_3$ solution for 10 s and then in 1 mM $PtCl_4$ solution for 10 min.

verifies that the deposited Au NPs in the first dipping step facilitate the deposition of metallic Pt onto the Si substrate, leading to the formation of Au−Pt alloy. It might be expected that Au^{3+} and $PtCl_6^{2-}$ would be unstable and tend to reduce on the Si or ITO-glass surface. In particular, Au^{3+} can be reduced to form metallic Au on the Si surface but Au^{+} species on the ITO-glass surface, while $PtCl_6^{2-}$ can only be partially reduced to the Pt^{2+} state on both Si and ITO-glass surfaces. In contrast, both Au^{3+} and $PtCl_6^{2-}$ ions when present in the same solution are found to reduce to Au−Pt alloy on the Si surface but not the ITO-glass surface.

The Au−Pt alloy NPs prepared in the present simple method can be used as effective catalysts. In Figure 6, we show the CV

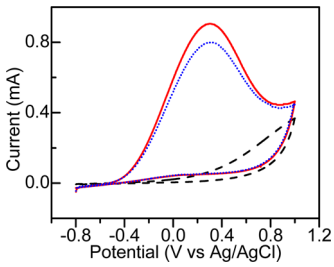

Figure 6. Cyclic voltammetric curves for the as-prepared Au−Pt alloy nanoparticles on a H-terminated Si substrate in 0.5 M KOH with (solid curve for 1st scan and dotted curve for the 50th cycle) and without (dashed curve) 0.5 M methanol at 10 mV/s.

curves of the Au−Pt NPs on a H-terminated Si substrate in a solution of 0.5 M KOH with and without 0.5 M methanol. Evidently, the CV curve reveals no peaks in the absence of methanol. However, when methanol is present, a peak at 0.29 V corresponding to the electrocatalytic oxidation of methanol is clearly observed. Even after 50 cycles, the methanol electro-oxidation peak is found to remain at the same potential, but with the current reduced slightly by 12%. The present work has therefore provided a simple way to prepare the Au−Pt alloy NPs, which, as we demonstrate here, can be used as a powerful electrocatalyst and also as a selective oxidant and dehydrogenation catalyst. Furthermore, by dipping the Si substrate in a solution of 1 mM $AuCl_3$ and 1 mM $PtCl_4$ for a much shorter time of 1 s, the average size of the spherical Au−Pt alloy NPs can be reduced to 6 nm, which shows that it is feasible to control the NP size easily below 10 nm by manipulating the dipping time. The corresponding alloy composition as estimated from XPS data (not shown) is found to be $Au_{98}Pt_2$.

4. CONCLUSIONS

Au−Pt alloy nanoparticles have been obtained on a H-terminated Si(100) substrate by an extremely simple method of dip-coating in a solution of 1 mM $AuCl_3$ and 1 mM $PtCl_4$. Scanning electron microscopy shows that these spherical NPs are 10 nm in average size. X-ray photoelectron spectroscopy clearly reveals that the Au $4f_{7/2}$ feature at 83.9 eV and Pt $4f_{7/2}$ feature at 70.6 eV of these NPs are both shifted to a lower binding energy compared to those of metallic Au and Pt, confirming the formation of Au−Pt alloy. Glancing-incidence X-ray diffraction also shows that the Au−Pt NPs exhibit a single-crystalline face-centered cubic alloy phase. We also demonstrate that the as-prepared Au−Pt alloy NPs can be used as a powerful catalysis for methanol oxidation, making the present method the simplest method to prepare anode electrodes for fuel cell applications.

AUTHOR INFORMATION

Corresponding Author

*E-mail: tong@uwaterloo.ca.

Notes

The authors declare no competing financial interest.

ACKNOWLEDGMENTS

This work is supported by the Natural Sciences and Engineering Research Council of Canada.

REFERENCES

(1) Mirdamadi-Esfahani, M.; Mostafavi, M.; Keita, B.; Nadjo, L.; Kooyman, P.; Remita, H. Bimetallic Au-Pt Nanoparticles Synthesized by Radiolysis: Application in Electro-Catalysis. *Gold Bull.* **2010**, *43*, 49−56.

(2) Abdelsayed, V.; Aljarash, A.; Samy El-Shall, M.; Al Othman, Z. A.; Alghamdi, A. H. Microwave Synthesis of Bimetallic Nanoalloys and CO Oxidation on Ceria-Supported Nanoalloys. *Chem. Mater.* **2009**, *21*, 2825−2834.

(3) Hernández-Fernández, P.; Rojas, S.; Ocón, P.; Gómez de la Fuente, J. L.; San Fabián, J.; Sanza, J.; Peña, M. A.; García-García, F. J.; Terreros, P.; Fierro, J. L. G. Influence of the Preparation Route of Bimetallic Pt−Au Nanoparticle Electrocatalysts for the Oxygen Reduction Reaction. *J. Phys. Chem. C* **2007**, *111*, 2913−2923.

(4) Luo, J.; Njoki, P. N.; Lin, Y.; Mott, D.; Wang, L. Y.; Zhong, C. J. Characterization of Carbon-Supported AuPt Nanoparticles for Electrocatalytic Methanol Oxidation Reaction. *Langmuir* **2006**, *22*, 2892−2898.

(5) Lang, H. F.; Maldonado, S.; Stevenson, K. J.; Chandler, B. D. Synthesis and Characterization of Dendrimer Templated Supported Bimetallic Pt−Au Nanoparticles. *J. Am. Chem. Soc.* **2004**, *126*, 12949−12956.

(6) Takatani, H.; Kago, H.; Nakanishi, M.; Kobayashi, Y.; Hori, F.; Oshima, R. Characterization of Noble Metal Alloy Nanoparticles Prepared by Ultrasound Irradiation. *Rev. Adv. Mater. Sci.* **2003**, *5*, 232−238.

(7) Hultgren, R.; Desai, P. D; Hawkins, D. T.; Gleiser, M.; Kelley, K. K. *Selected Values of the Thermodynamic Properties of Binary Alloys*; American Society for Metals: Metals Park, OH, 1973.

(8) Xiao, S.; Hu, W.; Luo, W.; Wu, Y.; Li, X.; Deng, H. Size Effect on Alloying Ability and Phase Stability of Immiscible Bimetallic Nanoparticles. *Eur. Phys. J. B* **2006**, *54*, 479−484.
(9) Schrinner, M.; Proch, S.; Mei, Y.; Kempe, R.; Miyajima, N.; Ballauff, M. Stable Bimetallic Gold−Platinum Nanoparticles Immobilized on Spherical Polyelectrolyte Brushes: Synthesis, Characterization, and Application for the Oxidation of Alcohols. *Adv. Mater.* **2008**, *20*, 1928−1933.
(10) Xu, J. B.; Zhao, T. S.; Liang, Z. X.; Zhu, L. D. Facile Preparation of AuPt Alloy Nanoparticles from Organometallic Complex Precursor. *Chem. Mater.* **2008**, *20*, 1688−1690.
(11) Habrioux, A.; Vogel, W.; Guinel, M.; Guetaz, L.; Servat, K.; Kokoh, B.; Alonso-Vante, N. Structural and Electrochemical Studies of Au−Pt Nanoalloys. *Phys. Chem. Chem. Phys.* **2009**, *11*, 3573−3579.
(12) Essinger-Hileman, E. R.; DeCicco, D.; Bondi, J. F.; Schaak, R. E. Aqueous Room-Temperature Synthesis of Au-Rh, Au-Pt, Pt-Rh, and Pd-Rh Alloy Nanoparticles: Fully Tunable Compositions within the Miscibility Gaps. *J. Mater. Chem.* **2011**, *21*, 11599−11604.
(13) Kern, W., Ed. *Handbook of Semiconductor Wafer Cleaning Technology*; Noyes: Park Ridge, NJ, 1993.
(14) Zhao, L. Y.; Leung, K. T. To be published.
(15) Vegard, L. Z. Die Konstitution der Mischkristalle und die Raumfüllung der Atome. *Z. Phys.* **1921**, *5*, 17−26.
(16) Cullity, B. D. *Elements of X-ray Diffraction*, 2nd ed.; Addison-Wesley: Reading, MA, 1978; p 102.
(17) Cho, B. O.; Chang, J. P.; Min, J. H.; Moon, S. H.; Kim, Y. W.; Levin, I. Material Characteristics of Electrically Tunable Zirconium Oxide Thin Films. *J. Appl. Phys.* **2003**, *93*, 745−749.
(18) Bastl, Z.; Pick, Š. Angle Resolved X-ray Photoelectron Spectroscopy Study of Au Deposited on Pt and Re Surfaces. *Surf. Sci.* **2004**, *566−568*, 832−836.
(19) Ge, X. B.; Yan, X. L.; Wang, R. Y.; Tian, F.; Ding, Y. Tailoring the Structure and Property of Pt-Decorated Nanoporous Gold by Thermal Annealing. *J. Phys. Chem. C* **2009**, *113*, 7379−7384.
(20) Xu, C. X.; Wang, R. Y.; Chen, M. W.; Zhang, Y.; Ding, Y. Dealloying to Nanoporous Au/Pt Alloys and Their Structure Sensitive Electrocatalytic Properties. *Phys. Chem. Chem. Phys.* **2010**, *12*, 239−246.
(21) Novak, I. The Photoelectron Spectroscopy of Organic Derivatives of Gold and Silver. In *The Chemistry of Organic Derivatives of Gold and Silver*; Patai, S., Rappoport, Z., Eds.; John Wiley & Sons, Ltd.: Chichester, U.K., 1999; Chapter 5, pp 103−129.
(22) Zhao, L. Y.; Siu, A. C. -L.; Petrus, J. A.; He, Z. H.; Leung, K. T. Interfacial Bonding of Gold Nanoparticles on a H-terminated Si(100) Substrate Obtained by Electro- and Electroless Deposition. *J. Am. Chem. Soc.* **2007**, *129*, 5730−5734.
(23) Gómez de la Fuente, J. L.; Martínez-Huerta, M. V.; Rojas, S.; Terreros, P.; Fierro, J. L. G.; Peña, M. A. Methanol Electrooxidation on PtRu Nanoparticles Supported on Functionalised Carbon Black. *Catal. Today* **2006**, *116*, 422−432.
(24) Salzemann, C.; Petit, C. Influence of Hydrogen on the Morphology of Platinum and Palladium Nanocrystals. *Langmuir* **2012**, *28*, 4835−4841.